Plasmonics (2009) 4:281–292
DOI 10.1007/s11468-009-9104-4

Theoretical and Experimental Investigation of Enhanced Transmission Through Periodic Metal Nanoslits for Sensing in Water Environment

Alina Karabchevsky · Olga Krasnykov · Mark Auslender · Benny Hadad · Adi Goldner · Ibrahim Abdulhalim

Received: 8 February 2009 / Accepted: 31 August 2009 / Published online: 18 September 2009

Abstract Experimental and theoretical study of sensors based on enhanced transmission through periodic metal nanoslits is presented. Our approach consists of the design of one-dimensional nanoslits array and its application in sensing for water quality control. Rigorous coupled waves analysis was used for the design and fit to the experimental data. Two types of surface plasmon resonance excitations are shown to be possible, one at the upper grating–analyte interface and one at the lower grating–substrate interface. This latter resonance is shown to be affected by the multiple interference or cavity-type effects. Those structures were fabricated by deposition of the metal layer and electron beam lithography of the nanostructure. We found that Ag-based periodic array exhibits the highest sensitivity to refractive index variations. Sensitivity enhancement was measured by ethanol concentrations in water. Stability of the Ag-based sensor was improved by covering the grating with less than 15 nm polymethyl methacrylate capping layer without deterioration of the sensitivity.

A. Karabchevsky (✉) · O. Krasnykov · I. Abdulhalim
Department of Electrooptic Engineering,
Ben Gurion University of the Negev,
Beersheba 84105, Israel
e-mail: rudenko@bgu.ac.il

M. Auslender
Department of Electrical and Computer Engineering,
Ben Gurion University of the Negev,
Beersheba 84105, Israel

B. Hadad · A. Goldner
The Weiss Family Laboratory for Nanoscale Systems,
Ben Gurion University of the Negev,
P.O. Box 653, Beersheba 84105, Israel

Keywords Surface plasmon resonance · Gratings · Enhanced transmission · Biosensors · Metal nanoslits array

Introduction

The interdisciplinary field of biosensors has led to the increased interaction between physicists, chemists, biochemists, and engineers for faster development of novel electronic devices that can be utilized for a variety of applications including human health care and environmental monitoring. The coupling of biological molecules with electronics [1] holds the key to recent successful developments in the area of biosensors. Optical biosensing is a strongly active field of research due to the need for high-sensitivity, rapid, specific, and reliable biosensors both for environmental control and for medical diagnosis. First optical sensors were based on the measurement of changes in absorption spectrum and were developed for the measurement of CO_2 and O_2 concentrations [2]. Nylander and Liedberg [3] demonstrated high-sensitivity sensing in the early 1980s using surface plasmon resonance (SPR) phenomenon. Since then, SPR phenomenon-based sensing has been receiving continuously growing attention [4]. In order to improve on an already successful panoply of optical biosensors, nano-photonic-structures composed of periodic metallic openings with dimensions less than the wavelength can be used. Within the periodic structures, quite unexpected phenomena emerge related to the existence of localized SPR (LSPR) and extended SPR excitations. One of the peculiar phenomena is the EROT, in which transmittance through such nano-openings, exceeds the relative area ratio (geometric limit) as predicted originally by Ebbesen et al. [5]. This result was mismatched with Bethe's aperture theory [6], which predicts negligible transmission through a single small

hole in a thin metal film; this phenomenon was termed *extraordinary optical transmission* (EOT). EOT causes large sensitivity because it involves two intertwined processes: (1) transmission through the nanoholes and (2) scattering of evanescent waves by the holes. Lee et al. [7, 8] demonstrated comparative study which verifies higher sensitivity of nanoslits over nanohole-based structures, and therefore nanoslits are better candidates for sensing designs. One of the applications of EOT phenomenon is sensing in water environment. Although Lee et al. were the first to report sensing in water using EOT in nanoslits, in this work, we report on a more extensive study where: (a) the effect of the different parameters on the sensor sensitivity was thoroughly studied; (b) the optimized sensor design in the visible spectral range is presented to get good contrast of the EOT peak, while in [7, 8] the resonance wavelength was in the near infrared; (c) use of silver instead of gold gives narrower EOT peak and therefore more accurate determination of the peak locations, hence better detection limit; (d) theoretical comparison between different nanoslit designs are carried out; (e) we report on experimental results of nonspecific sensing of organic chemicals such as methanol and ethanol, sugars such as sucrose and glucose, and large water pollutant such as *Escherichia coli* bacteria. We have shown for the first time the effect of the polymethyl methacrylate (PMMA) as a protective layer to the nanoslit-based sensor theoretically and experimentally. Field distribution calculations and EOT peak shift explain the sensitivity dependence on the PMMA thickness. In addition, the possible sensing of bacteria with nanoslits is presented, showing that there is a need for further study of this subject due to the large size of the bacteria as compared to the evanescence region.

By attaching molecules to the nanoslit structure, the transmission is modified significantly, and the overall transmission resonance undergoes a large shift in wavelength due to surface plasmons and cavity modes [9, 10]. There are several conditions for surface plasmon excitation, which depends on parameters such as angle of incidence, grating geometry, wavelength, and the dielectric constants of the metal and dielectrics below and above the grating. The resonance is observed in terms of a sharp dip in reflection or sharp peak in transmission in output optical signal at either resonance angle (angular interrogation) or resonance wavelength (spectral interrogation). Any change in refractive index near the interface causes a change in the value of the resonance location. This means that the resonance wavelength is sensitive to refractive index variations, a fact that makes this structure a potential sensor. In addition, periodically structured metallic films constituting of subwavelength apertures based on SPR phenomenon are potential sensors for variety of applications including water quality control. It remains unclear, however, whether this sensor is able to detect large biological or biochemical entities with dimensions larger than the slit width. A preliminary designed structure and methodology are proposed to allow sensing of large water pollutants such as *E. coli*. In food industry in general and in water industry in particular, quality of the product is evaluated by chemical (or microbiological) time-dependent analysis. Those processes include techniques such as: chromatography, spectrometry, electrophoresis, etc., which enable the recognition of water pollutants of small size and of little amounts. SPR-based optical biosensors have gained attention due to its speed of detection, high specificity, high sensitivity, and possibility of online real-time analysis [11]. Since the extraordinary transmission is a result of SPR, it is expected to have good surface sensitivity similar to conventional SPR sensors [8, 12]. Grating-based SPR devices show sensitivity of about 400 nm per refractive index unit (RIU) [10, 13].

In this work, our objective is to present optimum design of such structures as sensors for water quality control in the visible range with (1) high sensitivity to pollutants and (2) appropriate stability of the sensor in water environment. For large biological entities, however, we observed that the shift in the EOT peak is sometimes not monotonic; hence, it will be impossible to use these sensors to detect entities much larger than the slit width. Also, the enhanced local field extends only to a range of about 50–100 nm from the slits; hence, it will not sense the whole volume of a bacteria cell. This problem is well known in the traditional prism-coupled SPR sensors even though extended SP waves have a relatively larger propagation length along the surface of the order of 1 μm [14]. Long-range SPR configurations were proposed [15] to resolve this problem. Sensor-based EOT strongly depends on the detailed structure of the nanomaterial. It is well known that the aperture size and type of the metallic nanostructures have different contributions in the extraordinary transmission [16–18]. However, according to Lee et. al [8], the width of nanoslits is not affecting the sensitivity of the sensor. In addition, Zhang and Noguez [19] found that plasmonic absorption that is one of the involved phenomenon strongly depends on the detailed structure of the nanomaterial. Our intention is to present broad theoretical investigation and experimental results of suitable periodically structured metal nanoslit array based on EOT phenomena for sensing in water environment. Table 1 summarizes the abbreviation used during the article.

Sensor design: relation between grating detailed structure and plasmonic phenomenon

Wide theoretical analysis based on rigorous coupled wave analysis is presented here for evaluating optimal grating-based nanostructure. Figure 1a shows the general structure

Table 1 Abbreviation list used during the article

Abbreviation	Description
BGU	Ben Gurion University of the Negrev
DI	Deionized water
EOT	Extraordinary optical transmission
EROT	Enhanced resonance optical transmission
LSPR	Localized surface plasmon resonance
PMMA	Polymethyl methacrylate
TM	Transverse magnetic
RCW	Rigorous coupled wave approach
RIU	Refractive index units
SEM	Scanning electron microscope
SP	Surface plasmon
SPR	Surface plasmon resonance
1st λ_{res}	Sensitive resonance in the gratings (nm)
2nd λ_{res}	Almost constant peak in the gratings (nm)
NI	Normal incidence
S	Substrate
M	Metal
Eff	Effective

and geometrical parameters of the nanoslit array. Due to the k vector matching condition of SPR existence $k_x=k_{sp}$:

$$\lambda_{\text{analytical}} \overset{NI}{=} \text{Re}\left\{\Lambda\sqrt{\frac{n_m^2\varepsilon_2}{n_m^2+\varepsilon_2}}\right\} \quad (1)$$

where $n_m=n_r+i\kappa$ is the complex refractive index of the metal, and ε_2 is dielectric constant of the analyte. EOT resonance is linear with the grating pitch (Λ) [7], and therefore the higher the pitch is, the longer are the wavelengths at which EOT resonances occur, as can be seen in the case of air analyte in Fig. 1b. Since the main purpose of this paper is to report optimal design in the visible range for the sensing in water environment, we calculated the resonance location variations with the grating period in water. Multiple resonance peaks are obtained, for example, in the range 450–1,100 nm, four resonances are observed as can be seen in Fig. 2a for the case of $\Lambda \geq 650\,nm$ and three resonance peaks in Fig. 1b. For lower pitch values, only two peaks are observed. The height and contrast of the peaks are highest for the one at the longest wavelength. Therefore, we investigate mainly the two most clear peaks (the one with the longest wavelength, which we call second λ_{res} and the next one which we call the first λ_{res}). In order to understand if these resonances are of SPR origin, we calculated $\lambda_{analytical}$ according to Eq. 1 and plotted both resonance locations and $\lambda_{analytical}$ vs. Λ (see Figs. 1c and 2b). The linear regression estimations in Figs. 1c and 2b exhibit good linear fit. The existence of the offset is partially due to the dispersion of the refractive indices which makes the curve slightly nonlinear. The first peak λ_{res} agrees very well with the calculated values from the analytic Eq. 1, $\lambda_{analytical}$. However, the second peak λ_{res} values, although linear with the pitch, do not agree with $\lambda_{analytical}$. This indicates that the first peak is an SPR peak while the second peak is not. However, when Eq. 1 is used with ε_2 equals that of the substrate, we surprisingly get good agreement as shown in Fig. 2c. This indicates that the second peak is also an SPR generated at the grating–substrate interface. We concentrate on two nanoslit periodic structures behavior when Λ=450 nm and Λ=500 nm because these values give resonance in the visible range. For a complete understanding of the sensor behavior with the grating parameters, we have performed simulations at fixed period but with variable line width and height. Both the height and width play a role by affecting the phase accumulation. Figure 3 shows theoretical transverse magnetic (TM) transmission spectra of the Ag grating on SiO_2 substrate. The grating is characterized by Λ=450 nm, when refractive index of dielectric material is close to that of water environment (n_1=1.333), showing changes of the first resonance location to space width variation W. Figure 3

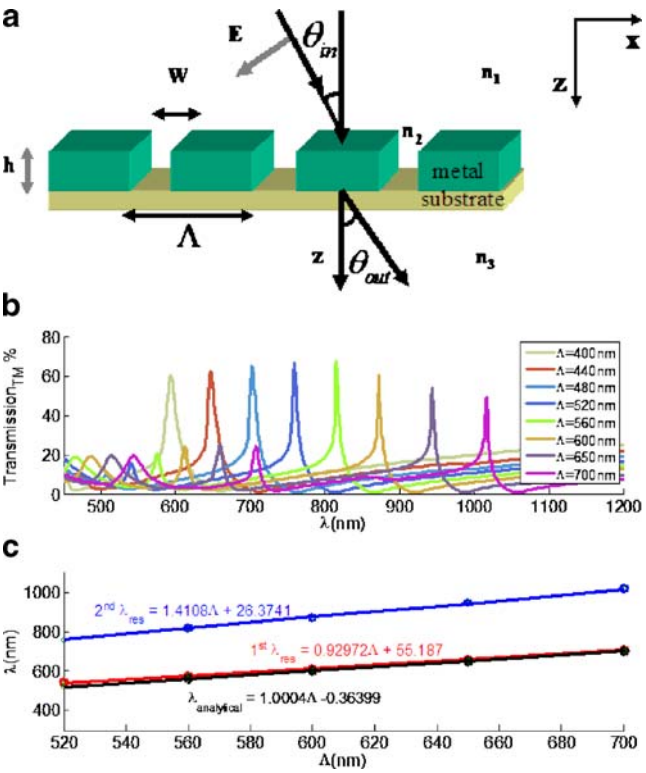

Fig. 1 **a** Periodic nanoslit geometry at any incidence angle and parameters considered in this work; **b** EOT spectra from silver-based gratings at normal incidence (θ_{in}=0) in air, for different grating periods Λ where n_1=1; n_3 is the refractive index of SiO_2 which is wavelength dependent, W=50 nm, h=60 nm; **c** resonance location vs. grating period showing the numerical (*dots*) and linear regression evaluation (*line*)

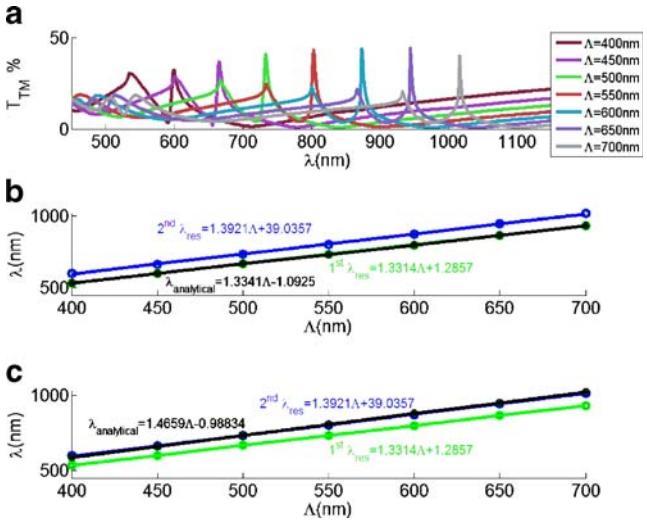

Fig. 2 **a** EOT spectra of Ag grating on SiO_2 substrate, where h= 45 nm, W=100 nm, n_1=1.333, and variable pitch; **b**, **c** resonance locations vs. grating period showing the numerical (*dots*) and linear regression evaluation (*line*), where in **b**, $\lambda_{analytical}$ was calculated using refractive index of analyte in Eq. 1, while in **c** it was calculated using refractive index of substrate

shows the effect of space width variations on the spectrum at different grating thicknesses. The shift of the first λ_{res} can be explained roughly according to the far-field approximation in which the diffraction is approximated by the Fourier transform. Within this approximation, the resonance location is linear with the slit width W. It can also be seen (in Fig. 3) that, with the enlargement of the aperture width W, more transmittance was allowed, showing enhancement of the resonant peak height. However, changes of the second λ_{res} are due to the change of grating period and thickness. Changes of the second peak are insignificant when metal thickness is 60 or 90 nm (Fig. 3c, d, respectively); however, when metal thickness is 30 or 45 nm, changes of the second peak became obvious (Fig. 3a, b, respectively).

Figure 4 shows theoretical TM transmission spectra of the Ag grating on SiO_2 substrate. The grating is characterized by Λ=500 nm, when the refractive index of the dielectric material (analyte) is close to that of water (n_1= 1.333), showing changes of the first λ_{res} to space width variation W at different thicknesses. As the metal thickness increases, the resonance peaks become more and more attenuated.

Figure 5 shows theoretical TM transmission spectra of the Ag grating on SiO_2 substrate where space width W varies for different grating periods at 45-nm metal thickness in water (n_1=1.333), showing changes of the first λ_{res}. It can be seen that higher period leads to second resonance transmission enhancement. Transmission of the first λ_{res} is almost constant with the period variation. All resonances move towards higher wavelengths when the period increases as expected.

Figure 6a shows the TM transmission spectra of the Ag grating characterized by 450-nm period, 70-nm slit width, and n_1=1.34 as a function of metal layer heights. Amplitude of transmission as a function of the wavelength of first resonance decreases with the metal thickness, indicating strengthening of absorption phenomena. The origin of the second peak, as we have shown above, is the excitation of an SPR at the grating–substrate interface; however, to excite this SPR properly, some conditions on the grating height and refractive indices need to be fulfilled. Since the grating acts as a cavity, interference effects lead to transmission peaks (cavity modes) which excite the SPR. This is supported by the fact that it shifts upon changing the grating height (Fig. 6b) but almost has no sensitivity to the

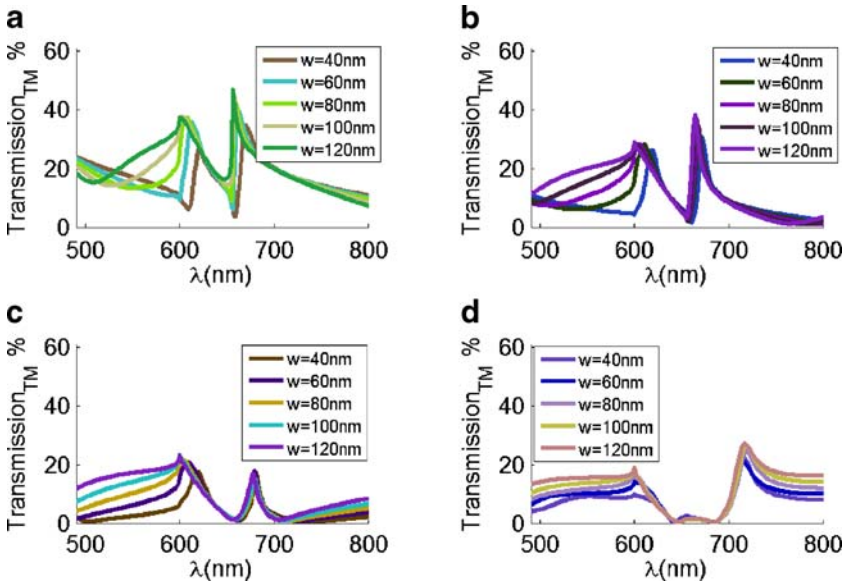

Fig. 3 EOT spectra of Ag grating on SiO_2 substrate where Λ=450 nm, n_1=1.333, **a** h= 30 nm, **b** h=45 nm, **c** h=60 nm, **d** h=90 nm where slit width W varied in all subplots

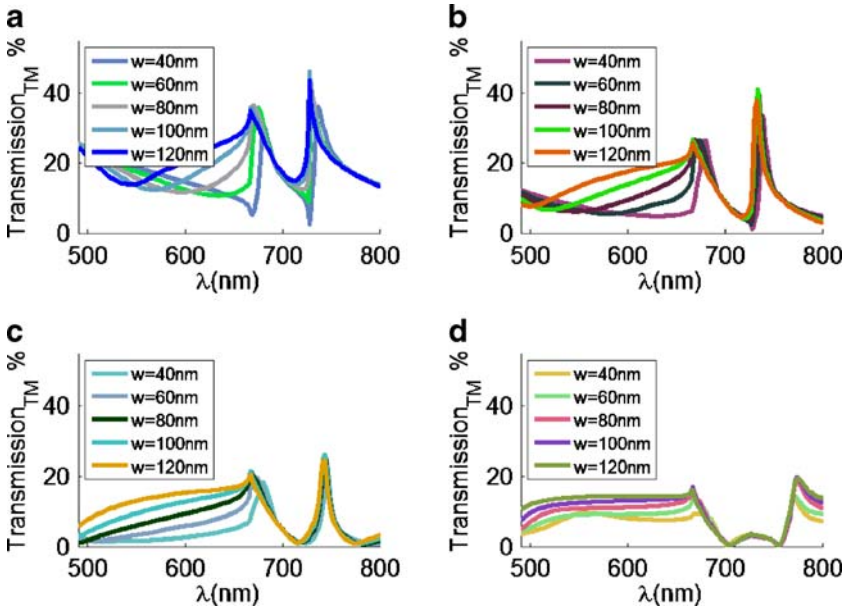

Fig. 4 **a**–**d** EOT spectra of Ag grating on SiO_2 substrate where Λ=500 nm, n_1=1.333, **a** h=30 nm, **b** h=60 nm, **d** h=90 nm where slit width W varied in all subplots

analyte index (Fig. 7a). The second peak also varies with the substrate refractive index as it is shown in Fig. 8. Hence, the phase accumulation during roundtrip in the cavity affects the second peak height and position. This might explain the larger offset seen in the linear fit in Fig. 2c.

In order to try and verify this proposition, we consider a cavity of height h filled with metal of effective index n_{eff} on substrate with index n_s. From the phase matching condition for a cavity mode, we arrived to the following relation:

$$\lambda = \frac{4\pi h \mathrm{Re}\{n_{\text{eff}}\}}{2m\pi - \varphi_{\text{Frenel}}} \tag{2}$$

Where at normal incidence, $\varphi_{\text{Frenel}} = \tan^{-1}\left\{\frac{\mathrm{Im}(r_{\text{ms}})}{\mathrm{Re}(r_{\text{ms}})}\right\}$ is Fresnel phase and $r_{\text{ms}} = \frac{n_s - n_m}{n_m + n_s}, R = |r_{\text{ms}}|^2$; r_{ms} is the reflectivity amplitude from the metal (m)–substrate (s) interface; n_{eff} is an effective refractive index of the metal grating layer that was calculated according to numerical (Fig. 6b, dots) result through the following equation:

$$\frac{\Delta\lambda}{\Delta h} = \frac{4\pi \mathrm{Re}\{n_{\text{eff}}\}}{2m\pi - \varphi_{\text{Frenel}}} \tag{3}$$

Linear regression to the numerical calculations of second λ_{res} vs. metal thickness (Fig. 6b) shows that the resonance location is a linear function as it is expected from the analytic expression of Eq. 2. From Fig. 6b, we have found

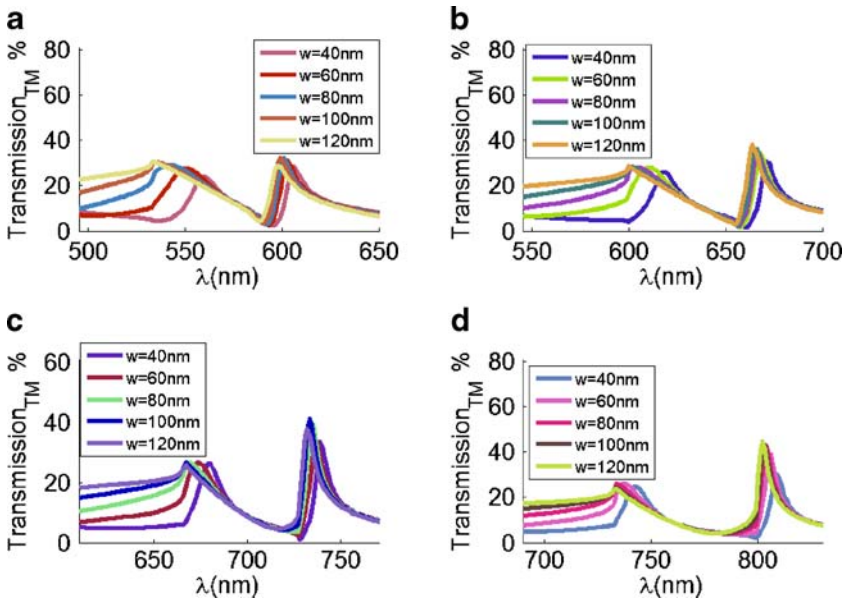

Fig. 5 EOT spectra of Ag grating on SiO_2 substrate where h=45 nm, n_1=1.333, **a** Λ=400 *nm*, **b** Λ=450 nm, **c** Λ=500 nm, **d** Λ=550 nm where slit width W varied in all subplots

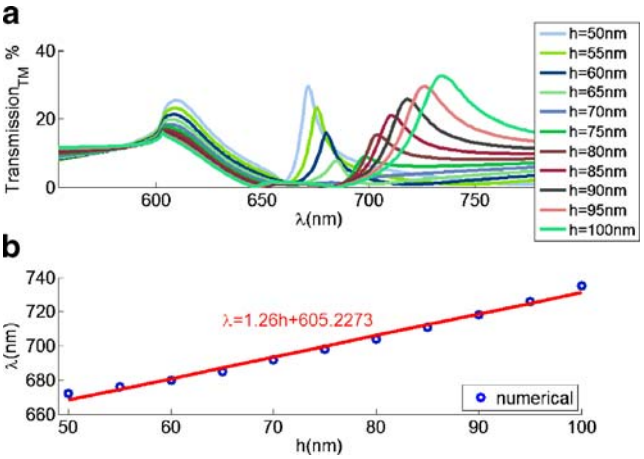

Fig. 6 **a** EOT spectra of the AG grating on SiO_2 substrate, where Λ=450 nm, W=70 nm, n_1=1.34, and h varies; **b** numerical results of second λ_{res} vs. metal thickness and linear regression evaluation (*line*)

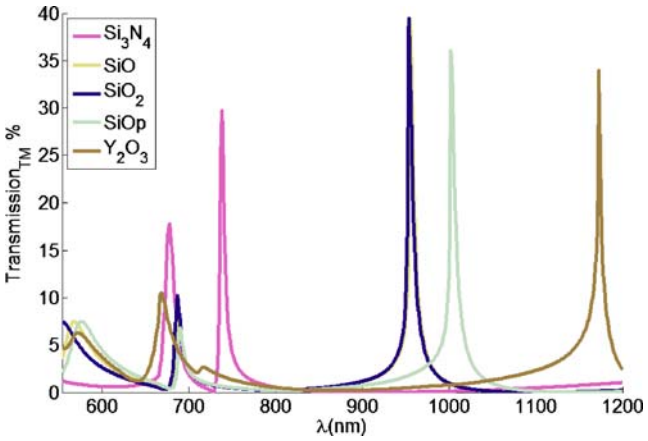

Fig. 8 EOT spectra of the Ag grating on different substrates, where Λ=500 nm, W=45 nm, n_1=1.333, and h=45 nm

that the slope of the line is $\Delta\lambda/\Delta h = 1.26$, and since the interference order is m=1, the effective refractive index is:

$$\mathrm{Re}\{n_{\mathrm{eff}}\} = \frac{1.26(2\pi - \varphi_{\mathrm{Frenel}})}{4\pi} \tag{4}$$

The value of n_{eff} depends on the wavelength and varies in the interval 0.56–0.57. In order to evaluate the effective index analytically, we used the expression based on the zero-order effective medium estimation. We calculated the effective index following Sobnak [20] et al. and found the value of 2.09 from the equation:

$$n_{\mathrm{eff}} = 1 + \frac{1}{2}\eta^2\left(1 + \sqrt{1 + \frac{4}{\eta^2}(1 + |\varepsilon_m|)}\right) \tag{5}$$

Where $\eta = \lambda/(\pi\omega|\varepsilon_m|)$. On the other hand, following Gordon [21], we found the value of 1.45 from the following equation:

$$\tanh\left(\sqrt{n_{\mathrm{eff}}^2 - 1}\,\frac{\pi w}{\lambda}\right) = -\frac{\sqrt{n_{\mathrm{eff}}^2 - \varepsilon_{\mathrm{m}}}}{\varepsilon_{\mathrm{m}}\sqrt{n_{\mathrm{eff}}^2 - 1}} \tag{6}$$

Our fit to the phase matching condition gives a value of 0.56–0.57. Hence, the conclusion is that both approaches are in fact not satisfactory. The reason is because both approaches consider the single slit as a metal waveguide problem, while our case includes periodic array of slits. In addition, Eqs. 5 and 6 describe air environment case while we are dealing with sensors for water environment. The fact that we obtained a value for n_{eff} less than 1 is also raising some doubts about the legitimacy of this approach. One problem could be with the calculation of the Fresnel phase

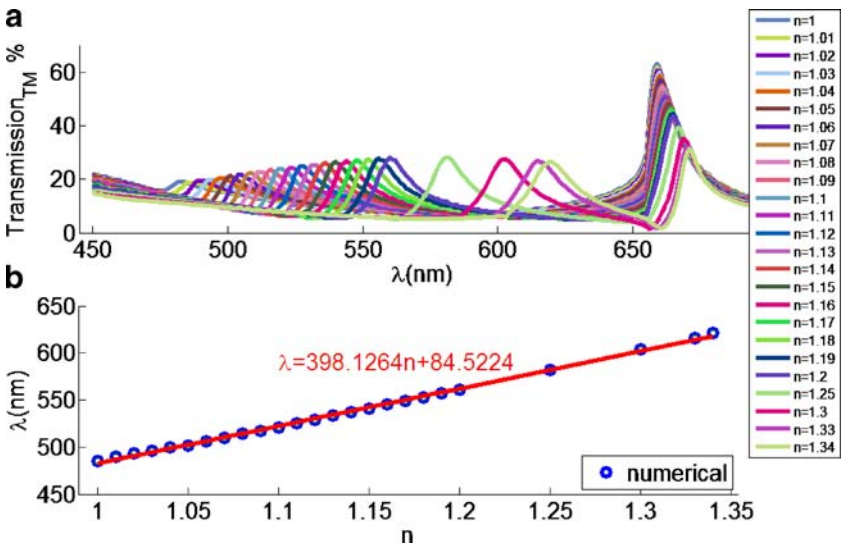

Fig. 7 **a** EOT spectra of the Ag grating on SiO_2 substrate with Λ=450 nm, W=45 nm, h=45 nm, where the refractive index of the analyte varies; **b** analytical (was calculated according to Eq. 1) and numerical results of the first resonance location vs. refractive index of the analyte n_1

Table 2 Summary of grating variables and their influence on resonance behavior

Variable (nm)	Sign	Action	1st λ_{res} (nm)	2nd λ_{res} (nm)
Period	Λ	Increasing	Shifts to higher λ	Nearly constant
Width	W	Increasing	Shifts to higher λ	Nearly constant
Metal height	h	Increasing	Shifts to lower λ	Shifts to higher λ

which we assumed was a plane wave reflection, while in fact the grating modes shape should be taken into account.

The offset of the linear plot is another parameter not explained by the analytic expression of Eq. 3. Perhaps higher-order approximations are required to estimate the effective index of the metal grating more precisely. Table 2 summarizes theoretical results presented in Figs. 3, 4, 5, and 6. Figure 7a shows the EOT spectra of the Ag grating characterized by Λ=450, W=45 nm, and h=45 nm on SiO_2 substrate, where the refractive indices of the dielectric (the analyte) vary. The resonance that appears at the shorter wavelengths side is sensitive to the refractive index variations (Fig. 7b), whereas the resonance that appears at the higher wavelengths is almost constant (the SPR cavity mode or substrate mode). This clearly points to the different origin of these peaks [22]. Note: the first λ_{res} was not observed during experimental results in air environment (n_1=1), probably because of the spectrometer range limitation. We found that the second λ_{res} is sensitive to the substrate index, as can be seen in Fig. 8 and as it is expected from a cavity mode. Therefore, we may call these resonances as *substrate modes*, although as we have shown previously they are cavity modes generating SPR at the grating–substrate interface.

Sensitivity (slope of the line in Fig. 7b) of refractive index sensors in the wavelength interrogation is defined in Eq. 7:

$$S = \frac{\Delta\lambda}{\Delta n}\left[\frac{\text{nm}}{\text{RIU}}\right] \tag{7}$$

Differentiating Eq. 1 with respect to the analyte refractive index n_1 gives an approximate numerical expression (Eq. 8) for the sensitivity of the grating (ignoring the dispersion).

$$\frac{d\lambda(n_1)}{dn_1} \overset{NI}{=} \Lambda \frac{\varepsilon_{mr}^{3/2}}{\left(\varepsilon_{mr} + n_1^2\right)^{3/2}} \tag{8}$$

However, metal height and slit width have to be taken into account for precise calculation of the periodic metal slit sensitivity as we have seen previously that they have some effect on the peak locations and its sensitivity. Sensitivity of Ag grating with 450-nm period, 45-nm slit width, and 45-nm thickness on SiO_2 substrate which can be calculated from the definition of grating sensitivity in Eq. 7 is approximately 398 nm/RIU (~3.98 nm/0.01, see Fig. 7b). The offset of the regression line might be a result of the effect of the interference expressed as an effect of the grating thickness on the peak location.

Silver-based grating sensors give good sensing results in the visible range, but they are corrosive in water environment. For this reason, such sensors should be covered by protection layer. Usually, sensors based on SPR phenomena excited by Kretschmann configuration are covered by gold protection layer [11]. Moreover, in biosensing applications, immobilization of antibodies can be made easily to gold surfaces [11] for specific sensing of biological analytes. Therefore, we covered the silver-based grating with thin layer of gold (d_{gold}=5 nm); however, peeling off of the protection layer was observed during a short period of time. Thicker gold layer caused the transmission and the sensitivity to drop significantly. Therefore, in our design, we looked for a cover layer that can increase the stability to water environment of the silver-based grating and does not deteriorate the transmission and the sensitivity. A material with high potential we found is PMMA, which is an amorphous, colorless, and high-transparency polymer. Remarkable properties of PMMA are: strength, stiffness, durability to erosion, and corrosion [23], and in addition PMMA provides protection against thermal degradation [24]. Therefore, covering the periodic nanoslits with thin layer (≤15 nm) of PMMA improves stability of the sensor. Since the influence of PMMA protection layer on sensitivity of the grating was never examined before, we simulated the effect of the cover height d of the PMMA on the performance of the grating sensor (d_{PMMA}). Figure 9a illustrates the ideal structure that one may wish to have in which the PMMA layer covers the grating lines, spaces, and walls evenly. Practically, this is difficult to achieve due to viscosity of PMMA, and therefore we applied a PMMA layer that fills the spaces and covers the lines. As a result of minimizing the thickness of the PMMA layer, a valley is formed on top of the spaces as shown schematically in Fig. 9b. Since metal nanoslits have trapezoidal shape (see Fig. 9b) because of the lithographic techniques of its manufacture, we investigated whether its shape influences the resonance locations of the sensor. Figure 10a presents the results of EOT spectra through such structure of silver-based grating covered with PMMA in water environment showing that as the PMMA thickness increases, the first EOT resonance location shifts toward higher wavelengths.

In Fig. 10b, we show that the EOT zoomed on the first resonance location spectra of the suitable Ag grating when

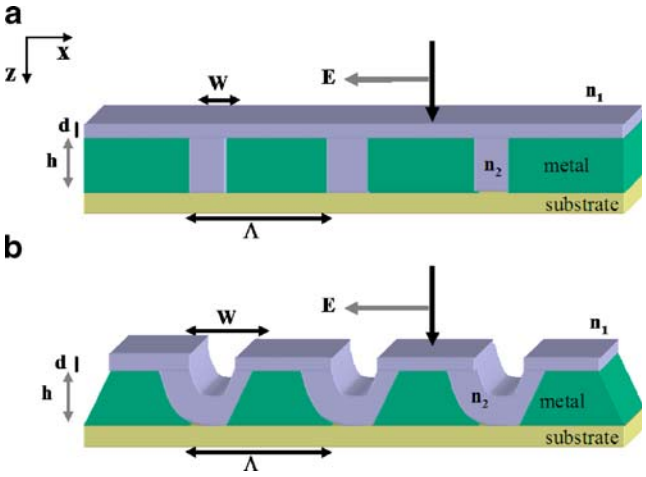

Fig. 9 Periodic nanoslit geometry based on EOT at normal incident (θ_{in}=0). **a** An ideal structure covered by PMMA of the thickness d. **b** Trapezoidal shape lines geometry and valley of PMMA

cover layer thickness varies, showing that, for thicknesses of $d_{PMMA} \leq 15$ nm, sensitivity is 4 nm/0.01=400 RIU; however, when the thicknesses increase (d_{PMMA}=15 nm), sensitivity decreases to 3 nm/0.01=300 RIU. As was mentioned above, instead of ideal straight nanoslits, the trapezoidal shape lines are received due to the lithographic processes (see Fig. 10b). We examined these unique forms of the lines. Figure 11 demonstrates EOT spectra of suitable Ag grating, when grating nanoslits are of trapezoidal shape for the 450-nm period (Fig. 11a) and 500-nm grating (Fig. 11b). From this simulation, it can be seen that trapezoidal shape of the grating line does not influence the resonance location. Once the grating structure is optimized in terms of spectral range of interest, transmission, sensitivity, and stability, the design was transferred to nanofabrication center for production.

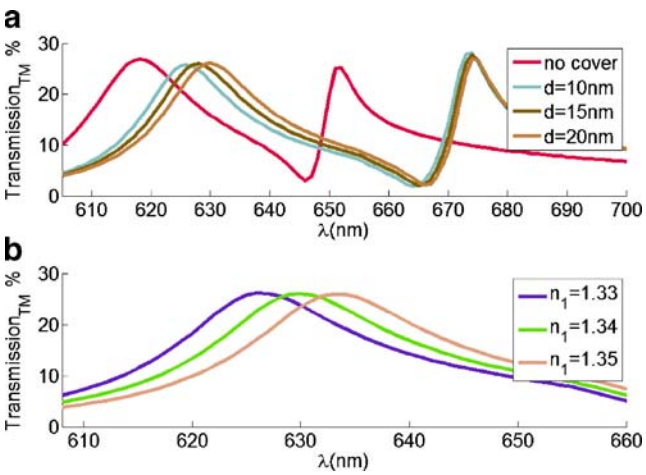

Fig. 10 EOT spectra of the Ag grating on SiO_2 substrate: **a** Λ=450 nm, W=45 nm, h=45 nm, n_1=1.34, and thickness $d_{PMMA950}$ layer is varied; **b** EOT zoomed on first λ_{res} of the Ag grating on SiO_2 substrate, where Λ=450 nm, W=45 nm, h=45 nm $d_{PMMA495}$=20 nm, when refractive index of the analyte varies

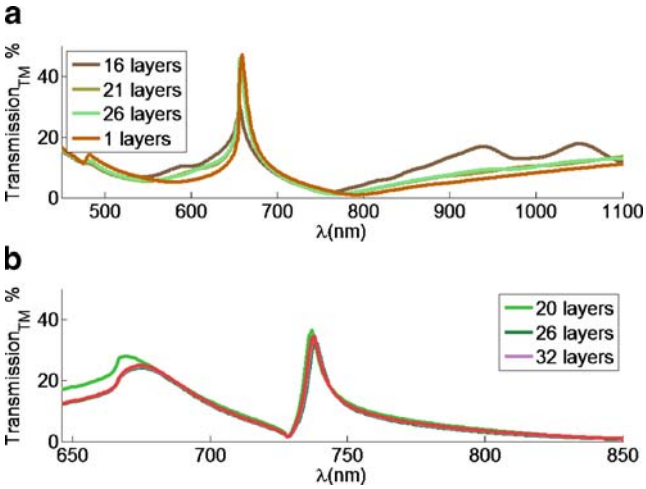

Fig. 11 EOT spectra of the Ag grating covered by PMMA950 protection layer on SiO_2 substrate, where **a** Λ=450 nm, W=45 nm, h=45 nm, n_1=1.34; **b** Λ=500 nm, W=100 nm, h=45 nm, n_1=1.333 when varying the number of layer slices composing the trapezoidal shape of the nanoslits

Grating fabrication

Synthesis or fabrication of metal structures based on either chemical or physical techniques was recently reviewed by Zhang and Noguez [19]. In this study, fabrication involves deposition of the metal layer and electron beam lithography for nanostructure patterning. We deposit Ag on a silica substrate using electron gun system with deposition rate of 0.6 A/s. After Ag deposition, we spin a thin layer of PMMA and bake it for 3 min at 180 °C. For the electron beam writing, done by e-line system of Raith, we use 20 keV with low current. The system writes 2-mm line long without stitching using Fix Beam Moving Stage mode. After writing, we develop the PMMA using MIBK: IPA 1:3 for 45 s at 22 °C. For etching the Ag lines, we use the PMMA as a mask and etch by ion beam milling for 4 min. The last stage of sensor fabrication included spinning of the PMMA (<15-nm thickness) on Ag grating surface for encapsulation.

Table 3 summarizes the structures fabricated and tested. Figure 12 shows some of their SEM micrographs. Note that the lines do not have straight walls but rather trapezoidal shapes. This is why the space width value usually is in the range of 50–100 nm with the bottom being closer to 50 nm while the top is closer to 100 nm. We have theoretically checked that the line profile does not have a significant effect on the resonance peaks nor on the sensor sensitivity (see design section, Fig. 11).

Table 3 Structures fabricated and tested in the study

Metal	Cover layer	h (nm)	W (nm)	d (nm)	Λ (nm)
Ag	–	45	50–100		500
Au	–	45	50–100		500
Ag	Au	45	50–120	5	500
Ag	PMMA	45	50–100	15	500

Experimental

To characterize the structure, a polarized reflection–transmission setup was built as shown in Fig. 13. The light source is a deuterium–halogen lamp coupled to a 0.6-mm-diameter core fiber. The light output at the distal end of the fiber is collimated with a lens, passing through a polarizer and through a pinhole of the same size as the sample and a beam splitter. The sample is held on an x–y rotating stage to allow best alignment to the beam and the polarizer. Analytes were dripped and pumped by digital micropipette. The transmitted and reflected beams are collected with a lens similar to the collimation lens and launched into an output fiber which is connected to the spectrometer. Transmission signals taken by spectrometer were processed by Matlab.

The ability of the different analyte recognition by designed structures was checked in the first stage of the research when our goal is the recognition of pollutants in water environment. Figure 14 shows transmission spectra of Ag grating sensor characterized by Λ=450 nm, W= 100 nm, and h=45 nm, showing changes in resonance location. This figure demonstrates nonsensitivity to the analyte variation. For this latter property, we propose the following: (1) antibodies need to be bound to the surface that specifically connects biological entities; (2) sensitivity can be increased by increasing the grating period; (3) large bacteria can be detected at high frequencies such as terahertz.

The refractive index sensitivity of the designed structure as a sensor was investigated using the organic analyte ethanol in deionized (DI) water because such mixtures have known refractive indices. DI water served as the reference. Figure 15a shows six EOT spectra measured with six ethanol diluted in DI compounds whose refractive indices are 1.333, 1.3395, 1.3469, 1.3535, 1.3583, and 1.3616, respectively [25, 26]. The first λ_{res} moves toward longer wavelengths with the increase of the compound index of refraction, evidencing the capability of the sensor to detect a small change in refractive index of the liquid. Figure 15a shows transmission spectra of the Ag-manufactured grating, when n_1 varies according to the ethanol diluted in DI compounds where the sensitive peak (first λ_{res}) is zoomed on Fig. 15b. Figure 15c illustrates wavelength as a function of the refractive index, showing the sensitivity of the structure as a slope of the trend line 349.4 nm/RIU.

Sensitivity of designed grating to organic analytes

Figure 16a shows EOT spectra of manufactured grating covered by PMMA protection layer, where the region of interest (the first λ_{res} location) is zoomed and presented in Fig. 16b, showing the shift of the first λ_{res} location towards higher wavelengths as a function of refractive index of analyte. Sensitivity of this design can be seen from wavelength vs. refractive index plot (Fig. 16c), showing enhancement (slope of the regression line: $S = 435.3[\mathrm{nm/RIU}]$) in

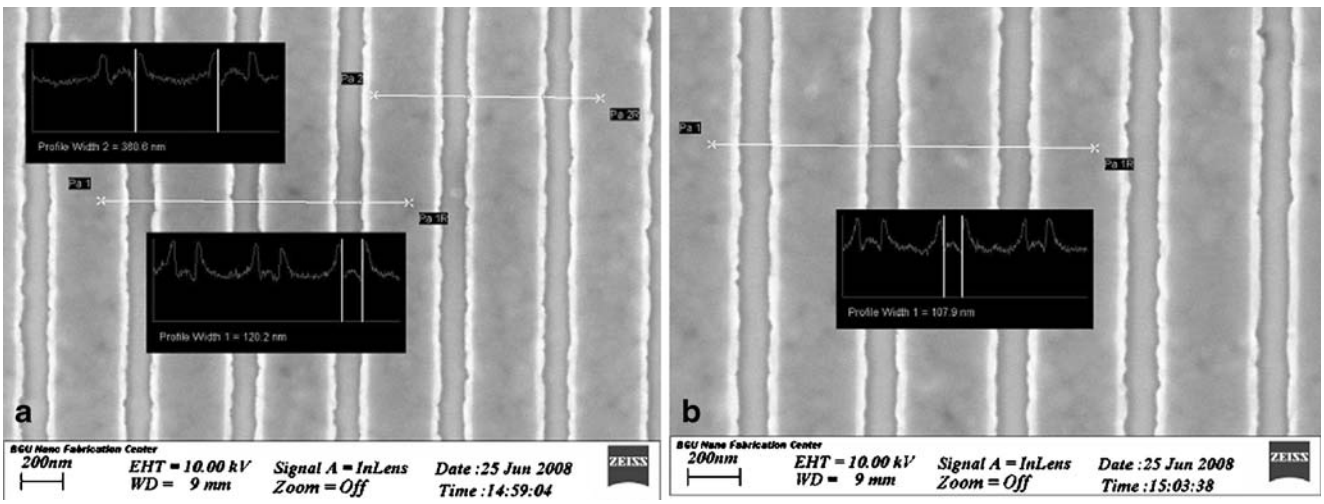

Fig. 12 Scanning electron microscope images of the Ag grating with the following parameters: Λ=500 nm, W=50–100 nm; h=45,200 nm scale. **a** Without cover layer; **b** grating covered by PMMA950

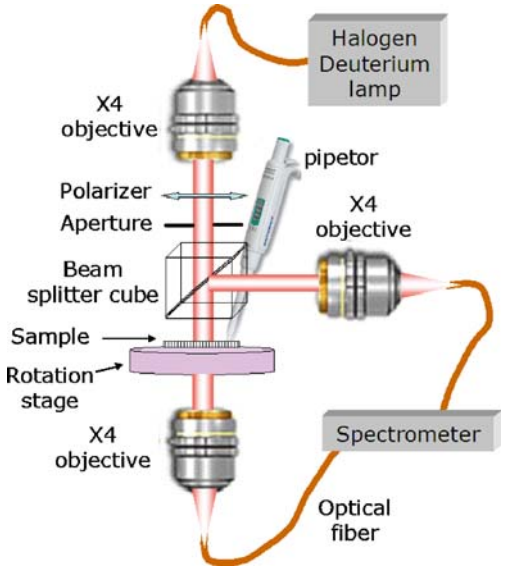

Fig. 13 Schematic of the experimental setup

sensitivity, relative to the case when the grating is covered by gold layer (Fig. 15c $S = 349.4[\mathrm{nm/RIU}]$) and relative to the case without PMMA layer ($S = 398[\mathrm{nm/RIU}]$). Enhancement of the measured sensitivity of the fabricated sensor covered with PMMA could be a result of small deviation of the grating parameters from the design. Sensitivity as was discussed above can increase, for example, by increasing the pitch of the sensor. This fact explains enhancement of the sensor which was designed by Karabchevsky et. al [13]. One of our findings is that the sensitivity is not affected by the addition of less than or equal to 15-nm PMMA layer as can be seen form Fig. 17a (left axis). Penetration depth defined as the distance at which the field arrives to $1/e$ of its value at the interface is larger for the case of grating covered by PMMA than the case without PMMA, and therefore sensitivity of the grating with PMMA should increase

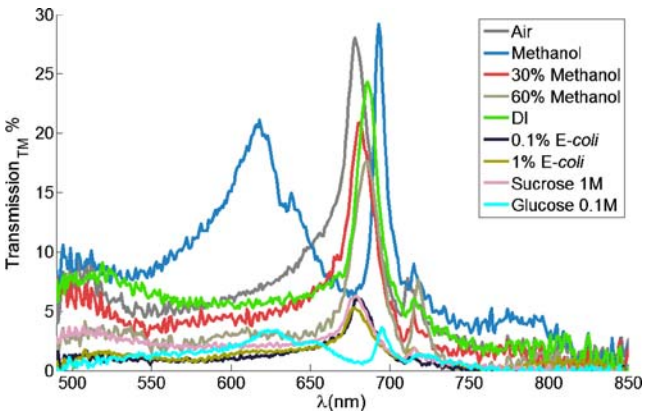

Fig. 14 Experimental results: EOT spectra of Ag grating as a function of wavelength from variety of analytes

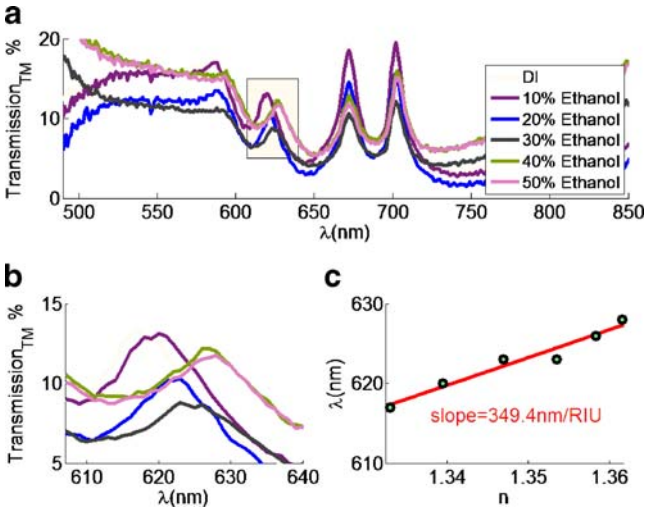

Fig. 15 Experimental results. **a** Transmission spectra of the Ag grating covered by d_{Au}=5 nm, for different analytes composed of ethanol diluted in DI water; **b** zoom on the gray area in the gray box of **a**; the legend is the same for **a** and **b**. **c** Wavelength as a function of refractive index of ethanol concentrations diluted in DI of resonance presented in **b** and its evaluated regression line

(Fig. 17b). In addition, resonance locations move towards higher wavelengths as a function of d_{PMMA} (Fig. 10a) and therefore, by increasing n_{eff}, should increase sensitivity. Since in case of grating with protection layer the sensitivity does not change, comparisons of penetration depths and observing behavior of resonance locations are not enough, and examination of electric energy should be done.

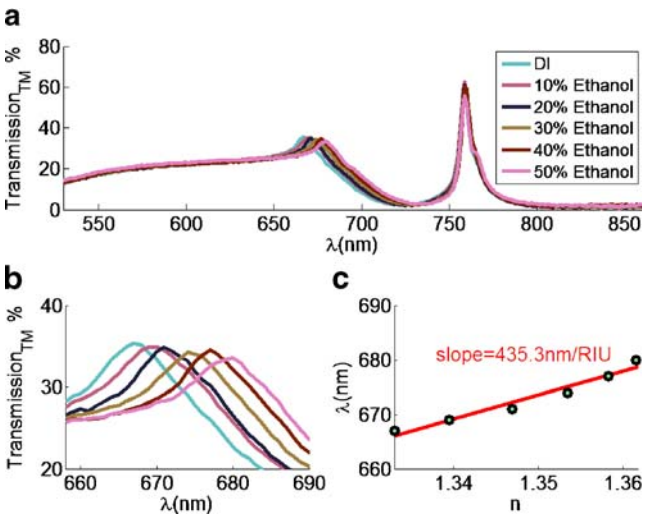

Fig. 16 Experimental results. **a** Transmission spectra of Λ=500 nm, W=45 nm, h=45 nm grating coated by $d_{\mathrm{PMMA}} \leq 15$ nm where changes of refractive index can be seen due to different concentrations of ethanol in DI water; **b** zoom on the lower wavelengths resonance that appears on a subplot, the legend is the same for the subplots **a** and **b**. **c** Wavelength as a function of refractive index of ethanol diluted in DI water and its evaluated regression line

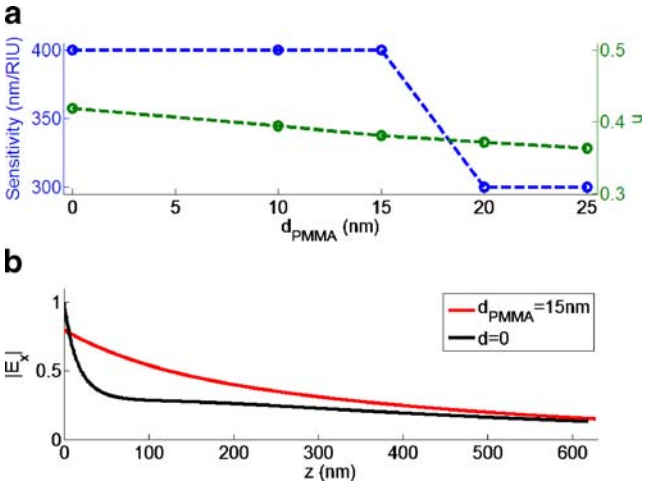

Fig. 17 **a** Sensitivity (*left axis*) normalized to its maximal value energy u according to Eq. 10 (*right axis*) vs. thickness of the PMMA layer; **b** absolute value of E_x along z direction in cases of d_{PMMA}= 15 nm (λ_{res}=628 nm) and grating without cover (λ_{res}=619 nm)

Normalized electric energy according to Eq. 10 decreases as PMMA thickness increases (Fig. 17a, right axis). The field distribution modification following the addition of top dielectric layer is related to the same phenomenon of long-range SPR; however, in our case, the PMMA thickness is much less than the substrate thickness [27].

It was found that adding a dielectric layer to the SPR sensor surface enhances the sensitivity due to enhancing the interaction between the evanescent field and the analyte. This phenomenon was observed recently by Lahav et. al. on prism-coupled surface-plasmon-based sensors when covered by 10 nm of Si layer [28, 29]. Apparently, in the case of LSPR, this phenomenon does not exist. To check this further, we calculated the electromagnetic field distribution at resonance wavelength (first λ_{res}) within the analyte. Figure 18 shows the distribution of the electric energy density:

$$U(x,z) = |E_x|^2 + |E_z|^2 \tag{9}$$

for the cases where there are no cover and there is a 15-nm PMMA cover layer. Electric field components here are normalized to the incident field amplitudes. Distribution was calculated at the analyte domain which is the rectangular area [0 Λ]×[0 λ_{res}] where the top of the grating defines z=0. Note: here λ_{res} refers to the first λ_{res}. According to Floquet condition, solution of the wave equations in the x direction is periodic due to the periodic properties of the grating. For this reason, the electric energy values are calculated within one grating period according to Eq. 10. The choice of maximum z range is due to evanescent character of the calculated fields. It is seen from Fig. 18 that at the resonance wavelength there are some drastic variations of the energy density inside the area [0 Λ]×[0 λ_{res}]. Integration over the whole analyte volume is done according to Eq. 10, which describes normalized energy to the maximum value of the electric energy:

$$u = \frac{1}{\Lambda\lambda_{res}} \frac{\int_{x=0}^{\Lambda}\int_{z=0}^{\lambda_{res}} U dx dz}{\mathrm{Max}U_{x,z}} \tag{10}$$

At up to 15-nm thickness of PMMA layer, the energy is nearly constant and decreases above this thickness. For the case of 15 nm of PMMA, u is 0.3813, while for the case without PMMA, u is slightly higher at 0.419.

Conclusions

Metal nanoslit array was investigated for sensing in water, based on the extraordinary optical transmission. Parameters such as grating period, substrate, space width, origin and thickness of cover layer, metal thickness, and their effect on the sensor performance were studied. In water environment, two strong resonances are observed, while in air one of them (the lower wavelength) shifts and becomes weak. Both theoretical calculations verified by experimental results have indicated that the first resonance origin is in the plasmonic phenomenon at the grating–analyte interface which strongly depends on the structural properties of the sensor based on periodic nanoslits and EOT. This resonance was found highly sensitive to the changes of the analyte refractive index, and therefore sensitivity of the sensor was calculated from the sensitivity of its wavelength with the analyte index. However, the resonance located at higher wavelengths (second λ_{res}), the *substrate mode* or *SPR cavity mode*, occurs due to excitation of SPR at the grating–substrate interface affected by the multiple interferences of the cavity. Shift of the first resonance is line width

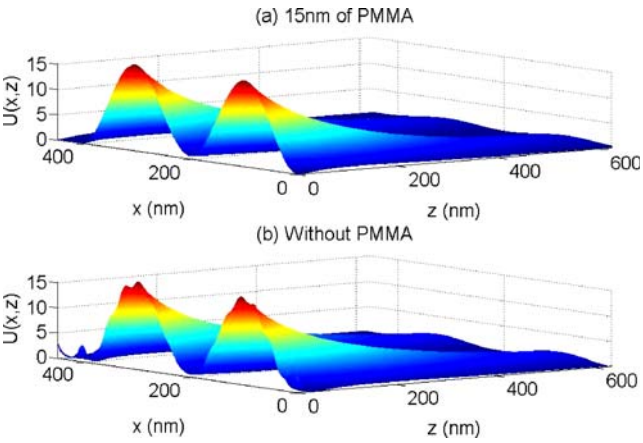

Fig. 18 Distribution of the electric energy density per RIU $U(x, z)$ of the grating where Λ=450 nm, W=45 nm, h=45 nm, n_1=1.34 when **a** d_{PMMA}=15 nm of PMMA where λ_{res}=628 nm; **b** grating without cover where λ_{res}=619 nm

dependent, a fact that can be explained roughly according to the far-field approximation. Simulation results show that nanoslit width does not affect the sensitivity of the sensor. Trapezoidal shape of the lines of manufactured gratings does not influence the resonance locations. Resonance wavelengths are highly dependent on the period of the grating and its metal layer height; therefore, these parameters have to be planned according to the type of the analyte and for the spectrometer range fitting. We found that the sensitivity of the sensor to the ethanol concentrations in water environment is 349 nm/RIU for Ag sensor covered by 5-nm gold layer; however, sensors covered by less than 15 nm of PMMA showed sensitivity of 435 nm/RIU experimentally and 398 nm/RIU theoretically. According to Fig. 17b, penetration depth of covered grating is higher. In addition, according to Fig. 10a, the resonance that was found sensitive to the changes of analyte moves towards the higher wavelengths as the PMMA thickness increases, and therefore the effective index increases. Hence, it seems that there are competing mechanisms affecting the sensitivity as the PMMA thickness increases, one which is the increase of the effective index causing the sensitivity of the sensor to increase and the other the decrease of the electromagnetic energy within the analyte which causes sensitivity to decrease. Neither the higher penetration depth condition nor the total electromagnetic energy is enough for estimating the sensitivity of the structure. For these reasons, the sensor with 15-nm PMMA cover does not show degradation in sensitivity. In addition, the PMMA cover layer improved stability of the sensor and prolonged its utilization.

Experimental results show that periodically structured metallic films constituting of subwavelength apertures based on SPR phenomenon have a potential as sensor for a variety of applications including water quality control. For large biological entities, however, we observed that the shift in the EOT peak is sometimes not monotonic; hence, it will be impossible to use these sensors to detect entities larger than or comparable to the slit width. Also, the enhanced local field extends only to a maximum range of about 300 nm (half the wavelength) from the slits; hence, it will not sense the whole volume (~1 μm) of a bacteria cell. Therefore, it remains unclear, however, whether this sensor is able to detect large biological or biochemical entities with dimensions larger than the slit width. However, designed structures at high frequencies such as terahertz can enable sensing of large bacteria such as *E. coli*.

Acknowledgements This work is supported by the Israeli Ministry of Science under the "Tashtiot" funding program. The help of Mr. Evgeni Eltzov and Prof. Robert Marks in the preparation of the biological samples is highly appreciated.

References

1. Arya Sunil K, Chaubey A, Malhotra BD (2006) Proc Indian Natn Sci Acad 72(4):249–266
2. Lubbers DW, Opitz N (1975) Zeitschrift Für Naturforschung C 30:532–533
3. Liedberg B, Nylander C, Sundstrom I (1983) Sens Actuators 4:299–304
4. Homola J, Sinclair S, Gauglitz GY (1999) Sens Actuators B 54:3–15
5. Ebbesen TW, Lezec HJ, Ghaemi HF, Thio T, Wolff PA (1998) Nature 391:667–669
6. Bethe HA (1944) Phys Rev 66:163–182
7. Lee KL, Wang KL, Wei PK (2007) J Biomed Opt 12(4):044023. doi:10.1117/1.2772296
8. Lee KL, Wang KL, Wei PK (2008) Plasmonics 3:119–125
9. García-Vidal FJ, Lezec HJ, Ebbesen TW, Martín-Moreno L (2003) Phys Rev Lett 90:213901
10. Ma J, Liu S, Zhang D, Yao J, Xu C, Shao J, Jin Y, Fan Z (2008) J Opt A Pure Appl Opt 10:035002
11. Rajan S, Chand S, Gupta BD (2006) Sens Actu B 115:344
12. Brolo AG, Gordon R, Leathem B, Kavanagh KL (2004) Langmuir 20(12):4813–4815
13. Karabchevsky A, Krasnyakov O, Abdulhalim I, Hadad B, Goldner A, Auslender M, Hava S (2009) Photonics Nanostruct Fundam Appl. doi:10.1016/j.photonics.2009.05.001
14. Abdulhalim I, Zourob MD, Lakhtakia A (2008) Electromagnetics 28:214–242
15. Ding Y, Cao ZQ, Shen QS (2003) Opt Quantum Electron 35:1091–1097
16. Cao Q, Lalanne P (2002) Phys Rev Lett 88:057403. doi:0.1103/PhysRevLett.88.057403
17. Fan W, Zhang S, Minhas B, Malloy KL, Brueck RJ (2005) Phys Rev Lett 94:033902
18. Koerkamp KJ, Enoch S, Segerink FB, Van Hulst NF, Kuipers L (2004) Phys Rev Lett 92:183901
19. Zhang JZ, Noguez C (2008) Plasmonics 3:127–150
20. Sobnack MB, Tan WC, Wanstall NP, Preist TW, Sambles JR (1998) Phys Rev Lett 80:5667–5669
21. Gordon R (2006) Phys Rev B 73:153405. doi:10.1103/PhysRevB.73.153405
22. Pang Y, Genet C, Ebbesen TW (2007) Opt Commun 280:10–15. doi:10.1016/j.optcom.2007.07.063
23. Yang Q, Cai F, Zhao LR, Huang X (2008) Surf Coat Technol 203:606–609. doi:10.1016/j.surfcoat.2008.04.072
24. Chuai C, Almdal K, Jorgensen JL (2004) J Appl Polym Sci 91:609–620
25. Suzuki H, Sugimoto M, Matsui Y, Kondoh J (2006) Meas Sci Technol 17:1547–1552. doi:10.1088/0957-0233/17/6/036
26. Weast RC, Astle MJ (1979) CRC handbook of chemistry and physics. CRC Press, Boca Raton
27. Barnes WL, Dereux A, Ebbesen TW (2003) Nature 424:824–830. doi:10.1038/nature01937
28. Lahav A, Auslender M, Abdulhalim I (2008) Opt Lett 33:2539–2541
29. Lahav A, Shalabaney A, Abdulhalim I (2009) J Nanophotonics 3:031501